3. Interior penalty method for elasticity

Little or nothing has been said about the choice of the numerical fluxes. A choice that yields a consistent and symmetric discontinuous Galerkin method and at the same time optimal convergence rate is the Interior Penalty (IP) method original from Arnold [6]. A consistent non-symmetric discontinuous Galerkin method will also be derived in this chapter.

3.1. Weak form of interior penalty method

The interior penalty method takes the numerical fluxes equal to, [8, 13],

$$\hat{\boldsymbol{u}} = \left\{\boldsymbol{u}^h\right\} \qquad \text{on } \tilde{\Gamma} \cup \Gamma^N, \tag{3.1}$$

$$\hat{\boldsymbol{u}} = \boldsymbol{g}^D = \boldsymbol{0} \qquad \text{on } \Gamma^D, \tag{3.2}$$

$$\hat{\boldsymbol{\sigma}}\boldsymbol{n}_K = \left\{\mathbf{C} : \nabla^s \boldsymbol{u}^h\right\} \boldsymbol{n}_K - \boldsymbol{\mu} \left[\!\left[\boldsymbol{u}^h\right]\!\right] \qquad \text{on } \tilde{\Gamma} \cup \Gamma^D, \tag{3.3}$$

$$\hat{\boldsymbol{\sigma}}\boldsymbol{n}_K = \boldsymbol{g}^N \qquad \text{on } \Gamma^N, \tag{3.4}$$

where $\boldsymbol{\mu}$, which definition will be given later, penalizes the jump in displacement between elements, $\left[\!\left[\boldsymbol{u}^h\right]\!\right]$. For simplicity it has been considered that the prescribed displacement has a value of $\boldsymbol{0}$. Observe that the method is consistent, since substituting the real continuous solution $\boldsymbol{u}$ into the numerical fluxes $\hat{\boldsymbol{u}}$ and $\hat{\boldsymbol{\sigma}}$, $\boldsymbol{u}$ and $\boldsymbol{\sigma}$ are obtained,

$$\hat{\boldsymbol{u}} = \{\boldsymbol{u}\} = \boldsymbol{u} \qquad \text{on } \tilde{\Gamma} \cup \Gamma^N, \tag{3.5}$$

$$\hat{\boldsymbol{u}} = \boldsymbol{g}^D = \boldsymbol{0} \qquad \text{on } \Gamma^D, \tag{3.6}$$

$$\hat{\boldsymbol{\sigma}}\boldsymbol{n}_K = \{\mathbf{C} : \nabla^s \boldsymbol{u}\} \boldsymbol{n}_K - \boldsymbol{\mu} [\![\boldsymbol{u}]\!] = \mathbf{C} : \nabla^s \boldsymbol{u}\, \boldsymbol{n}_K = \boldsymbol{\sigma}\boldsymbol{n}_K \qquad \text{on } \tilde{\Gamma} \cup \Gamma^D, \tag{3.7}$$

$$\hat{\boldsymbol{\sigma}}\boldsymbol{n}_K = \boldsymbol{g}^N \qquad \text{on } \Gamma^N. \tag{3.8}$$

In order to obtain the weak form for the interior penalty method, the numerical fluxes are inserted in the general weak form of discontinuous Galerkin methods in equation (2.34). Before doing so, some properties for the average and jump operators will be introduced. For any $\boldsymbol{g} : \tilde{\Gamma} \to \mathbb{R}$ it holds,

$$\{\{\boldsymbol{g}\}\} = \{\boldsymbol{g}\} \qquad [\![\{\boldsymbol{g}\}]\!] = \boldsymbol{0} \qquad \text{on } \tilde{\Gamma}, \tag{3.9}$$

$$[\![[\![\boldsymbol{g}]\!]]\!] = \boldsymbol{0} \qquad \{[\![\boldsymbol{g}]\!]\} = [\![\boldsymbol{g}]\!] \qquad \text{on } \tilde{\Gamma}. \tag{3.10}$$

Inserting the corresponding numerical fluxes into equation (2.34) and using the above

properties yields,

$$\int_{\tilde{\Omega}} \nabla^s \boldsymbol{\omega}^h : \mathbf{C} : \nabla \boldsymbol{u}^h d\Omega + \int_{\tilde{\Gamma}} \left\{ \nabla^s \boldsymbol{\omega}^h : \mathbf{C} \right\} \boldsymbol{n}_K \cdot \left[\!\left[-\boldsymbol{u}^h \right]\!\right] d\Gamma - \int_{\tilde{\Gamma} \cup \Gamma^D} \left[\!\left[\boldsymbol{\omega}^h \right]\!\right] \cdot \left(\left\{ \mathbf{C} : \nabla^s \boldsymbol{u}^h \right\} \boldsymbol{n}_K - \boldsymbol{\mu} \left[\!\left[\boldsymbol{u}^h \right]\!\right] \right) d\Gamma = \int_{\tilde{\Omega}} \boldsymbol{\omega}^h \cdot \boldsymbol{f} d\Omega + \int_{\Gamma^N} \boldsymbol{\omega}^h \cdot \boldsymbol{g}^N d\Gamma. \tag{3.11}$$

Note in the second term of the left hand side of the equation that the integrals over Γ^N and Γ^D disappear. This is because $\hat{\boldsymbol{u}} = \boldsymbol{u}^h$ on Γ. The third term of the left hand side is only integrated over $\tilde{\Gamma} \cup \Gamma^D$, since the integral over Γ^N has been taken to the right hand side of the equation after considering $\hat{\boldsymbol{\sigma}} \boldsymbol{n}_K = \boldsymbol{g}^N$ on Γ^N. Given that $\boldsymbol{\omega}^h = \mathbf{0}$ on Γ^D, and rearranging, the weak form for the interior penalty method is finally obtained,

$$\int_{\tilde{\Omega}} \nabla^s \boldsymbol{\omega}^h : \mathbf{C} : \nabla^s \boldsymbol{u}^h d\Omega - \int_{\tilde{\Gamma}} \left\{ \nabla^s \boldsymbol{\omega}^h : \mathbf{C} \right\} \boldsymbol{n}_K \cdot \left[\!\left[\boldsymbol{u}^h \right]\!\right] d\Gamma - \int_{\tilde{\Gamma}} \left[\!\left[\boldsymbol{\omega}^h \right]\!\right] \cdot \left\{ \mathbf{C} : \nabla^s \boldsymbol{u}^h \right\} \boldsymbol{n}_K d\Gamma + \int_{\tilde{\Gamma}} \left[\!\left[\boldsymbol{\omega}^h \right]\!\right] \boldsymbol{\mu} \left[\!\left[\boldsymbol{u}^h \right]\!\right] d\Gamma = \int_{\tilde{\Omega}} \boldsymbol{\omega}^h \cdot \boldsymbol{f} d\Omega + \int_{\Gamma^N} \boldsymbol{\omega}^h \cdot \boldsymbol{g}^N d\Gamma, \tag{3.12}$$

being,

$$\boldsymbol{\mu} = \frac{\eta_K}{h_K} \boldsymbol{D}, \tag{3.13}$$

where η_K is a dimensionless parameter depending on which, the method will be stable or unstable. The second-order tensor $\boldsymbol{D}$ has dimensions to guarantee dimensional consistency and h_k is a measure of the element size with the dimension of length. Using the definition of $\boldsymbol{\mu}$, in equation (3.13), the weak form for the interior penalty method in equation (3.12) may also be written as,

$$\int_{\tilde{\Omega}} \nabla^s \boldsymbol{\omega}^h : \mathbf{C} : \nabla^s \boldsymbol{u}^h d\Omega - \int_{\tilde{\Gamma}} \left\{ \nabla^s \boldsymbol{\omega}^h : \mathbf{C} \right\} \boldsymbol{n}_K \cdot \left[\!\left[\boldsymbol{u}^h \right]\!\right] d\Gamma - \int_{\tilde{\Gamma}} \left[\!\left[\boldsymbol{\omega}^h \right]\!\right] \cdot \left\{ \mathbf{C} : \nabla^s \boldsymbol{u}^h \right\} \boldsymbol{n}_K d\Gamma + \int_{\tilde{\Gamma}} \left[\!\left[\boldsymbol{\omega}^h \right]\!\right] \frac{\eta_K}{h_K} \boldsymbol{D} \left[\!\left[\boldsymbol{u}^h \right]\!\right] d\Gamma = \int_{\tilde{\Omega}} \boldsymbol{\omega}^h \cdot \boldsymbol{f} d\Omega + \int_{\Gamma^N} \boldsymbol{\omega}^h \cdot \boldsymbol{g}^N d\Gamma. \tag{3.14}$$

On the left hand side of the expression four separate terms can be distinguished. The first term is the term appearing in continuous Galerkin methods. The second term can be seen as the part of the weak form giving symmetry to the method, the third gives consistency and the fourth stability. These ideas will be developed now.

3.2. Consistency and conservation properties of interior penalty method

It has been shown that the IP method is consistent since the used numerical fluxes have been proved to be consistent, see equations (3.5)–(3.8). A method is conservative if it is single valued over $\tilde{\Gamma} \cup \Gamma$, and this is the case for the IP. If it is consistent and conservative it is called adjoint consistent [8]. This has beneficial properties related the convergence rate, as will be seen in Section 3.7.

Consider now the following numerical fluxes,

$$\hat{\boldsymbol{u}} = \boldsymbol{u}^h_{\partial K} \qquad \text{on } \tilde{\Gamma} \cup \Gamma^N, \tag{3.15}$$

$$\hat{\boldsymbol{u}} = \boldsymbol{g}^D = \boldsymbol{0} \qquad \text{on } \Gamma^D, \tag{3.16}$$

$$\hat{\boldsymbol{\sigma}}\boldsymbol{n}_K = \left\{\mathbf{C} : \nabla^s \boldsymbol{u}^h\right\} \boldsymbol{n}_K - \boldsymbol{\mu} \left[\!\left[\boldsymbol{u}^h\right]\!\right] \qquad \text{on } \tilde{\Gamma} \cup \Gamma^D, \tag{3.17}$$

$$\hat{\boldsymbol{\sigma}}\boldsymbol{n}_K = \boldsymbol{g}^N \qquad \text{on } \Gamma^N. \tag{3.18}$$

Again consistency can be proved easily with the explained properties of the average and jump operators. Again for simplicity $\boldsymbol{g}^D$ is considered to be $\boldsymbol{g}^D = \boldsymbol{0}$. Introducing the new numerical fluxes in the general weak form of the discontinuous Galerkin methods in equation (2.34),

$$\int_{\tilde{\Omega}} \nabla^s \boldsymbol{\omega}^h : \mathbf{C} : \nabla^s \boldsymbol{u}^h d\Omega - \int_{\Gamma^o} \left[\!\left[\boldsymbol{\omega}^h\right]\!\right] \cdot \left\{\mathbf{C} : \nabla^s \boldsymbol{u}^h\right\} \boldsymbol{n}_K ds + \int_{\Gamma^o} \left[\!\left[\boldsymbol{\omega}^h\right]\!\right] \frac{\eta_K}{h_K} \boldsymbol{D} \left[\!\left[\boldsymbol{u}^h\right]\!\right] ds$$
$$= \int_{\tilde{\Omega}} \boldsymbol{\omega}^h \cdot \boldsymbol{f} d\Omega + \int_{\Gamma^N} \boldsymbol{\omega}^h \cdot \boldsymbol{g}^N ds. \tag{3.19}$$

A new consistent method is obtained, with the same weak form as the IP method but without what was called the symmetry term. The symmetry term is therefore not necessary for consistency. It is introduced to guarantee the symmetry of the resulting bilinear form, and therefore of the resulting stiffness matrix. This method will be called the non-symmetric (NS) discontinuous Galerkin method. See however that it is not adjoint consistent since the value of $\hat{\boldsymbol{u}}$ is not single valued over $\tilde{\Gamma}$. Some numerical examples will be given for this method in Section 3.7.

By changing from the numerical fluxes in equations (3.1)–(3.4), equation (3.3) to $\hat{\boldsymbol{\sigma}}\boldsymbol{n}_K = \left\{\mathbf{C} : \nabla^s \boldsymbol{u}^h\right\} \boldsymbol{n}_K$, a consistent method is obtained without the stability term. This term is therefore not necessary for consistency, however it is needed for stability.

3.3. Symmetry of the bilinear form

As seen in equation (2.35) the variational problem can be expressed as $B_h^{IP}\left(\boldsymbol{\omega}^h, \boldsymbol{u}^h\right)$. The symmetry property can be easily demonstrated by proving that,

$$B_h^{IP}\left(\boldsymbol{\omega}^h, \boldsymbol{u}^h\right) = B_h^{IP}\left(\boldsymbol{u}^h, \boldsymbol{\omega}^h\right). \tag{3.20}$$

Note that without the symmetry term the resulting expression would not be symmetric.

3.4. Stability

Stability is one of the most important issues for the IP method. As has been said in Section 2.5, stability as well as consistency, are required for convergence. However for the IP method stability is conditional, and can only be guaranteed a priori for very simple one dimensional cases, as will be seen in Section 3.7.

It has been seen the strain energy must be positive. Going back to the weak form of the IP method in equation (3.14), and substituting $\boldsymbol{u}^h$ by $\boldsymbol{\omega}^h$ it yields,

$$2U = \int_{\tilde{\Omega}} \nabla^s \boldsymbol{\omega}^h : \mathbf{C} : \nabla^s \boldsymbol{\omega}^h d\Omega - \int_{\tilde{\Gamma}} \left\{ \nabla^s \boldsymbol{\omega}^h : \mathbf{C} \right\} \boldsymbol{n}_K \cdot \left[\!\left[\boldsymbol{\omega}^h \right]\!\right] d\Gamma - \int_{\tilde{\Gamma}} \left[\!\left[\boldsymbol{\omega}^h \right]\!\right] \cdot \left\{ \mathbf{C} : \nabla^s \boldsymbol{\omega}^h \right\} \boldsymbol{n}_K d\Gamma + \int_{\tilde{\Gamma}} \left[\!\left[\boldsymbol{\omega}^h \right]\!\right] \frac{\eta_K}{h_K} \boldsymbol{D} \left[\!\left[\boldsymbol{\omega}^h \right]\!\right] d\Gamma. \quad (3.21)$$

The integral over $\tilde{\Omega}$ in equation (3.21) has a positive contribution to the strain energy as long as $\mathbf{C}$ is positive definite. The last term of the right hand side of equation (3.21), which was called the stability term, has also a positive contribution to the strain energy as long as $\boldsymbol{\mu} = \frac{\eta_K}{h_K} \boldsymbol{D}$ is positive definite. If the other interface elements were to be excluded the formulation would be stable, however it would not be consistent. The resulting method is called the interface element or penalty method which weak form is equal to,

$$\int_{\tilde{\Omega}} \nabla^s \boldsymbol{\omega}^h : \mathbf{C} : \nabla^s \boldsymbol{\omega}^h d\Omega + \int_{\tilde{\Gamma}} \left[\!\left[\boldsymbol{\omega}^h \right]\!\right] \frac{\eta_K}{h_K} \boldsymbol{D} \left[\!\left[\boldsymbol{\omega}^h \right]\!\right] d\Gamma = \int_{\tilde{\Omega}} \boldsymbol{\omega}^h \cdot \boldsymbol{f} d\Omega + \int_{\Gamma^N} \boldsymbol{\omega}^h \cdot \boldsymbol{g}^N d\Gamma. \quad (3.22)$$

Going now back to the IP method, and considering again equation (3.21), there are two other terms contributing to the strain energy. These are the second term, on the right hand side of the equation, providing symmetry, and the third term providing consistency to the method. The problem is that it cannot be concluded whether they have a positive contribution to the strain energy.

To determine the contribution of the two terms the discretized primal form for the IP method is considered, see Section 3.5. The stability condition in equation (2.47) is equivalent, after discretization, to guarantee that the resulting stiffness matrix is positive definite. However, only for the one dimensional case, and for meshes with equal element length and stiffness it has been possible to determine a η_K which guarantees stability, as will be seen in Section 3.7.

This result however, cannot be extrapolated to other cases. To guarantee stability, η_K will be required to be big enough to ensure that the resultant stiffness matrix is positive definite. But as η_K increases the conditioning of the matrix increases, leading to an ill conditioned matrix, very sensitive to round-off errors.

3.5. Discretization of the weak form

The approximate solutions, $\boldsymbol{u}^h$ and $\boldsymbol{\omega}^h$, and the spaces $\mathcal{U}^h$ and $\mathcal{W}^h$ have been defined in (2.11) and (2.13). The general definition of these spaces will be restricted in this case to,

$$\mathcal{U}^h := \left\{ \boldsymbol{u}^h \mid \boldsymbol{u}^h \in \left[L^2(\Omega) \right]^n, \boldsymbol{u}^h \in \left[H^1(\tilde{\Omega}) \right]^n, \boldsymbol{u}^h \in [P^p(K)]^n, \boldsymbol{u}^h = \boldsymbol{g}^D \text{ on } \Gamma^D \right\}, \quad (3.23)$$

$$\mathcal{W}^h := \left\{ \boldsymbol{\omega}^h \mid \boldsymbol{\omega}^h \in \left[L^2(\Omega) \right]^n, \boldsymbol{\omega}^h \in \left[H^1(\tilde{\Omega}) \right]^n, \boldsymbol{\omega}^h \in [P^p(K)]^n, \boldsymbol{\omega}^h = 0 \text{ on } \Gamma^D \right\}, \quad (3.24)$$

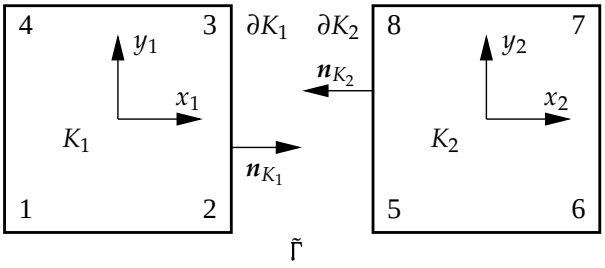

Figure 3.1. Two dimensions interface element.

where $P^p(K)$ is a finite dimensional space of polynomials of order p defined in each of the partitions K.

The weak form for the interior penalty method, equation (3.14), for the two dimensions interface elements in figure 3.1 will be discretized. The approximations used for $\boldsymbol{u}^h$, $\nabla^s \boldsymbol{u}^h$, $\boldsymbol{\omega}^h$ and $\nabla^s \boldsymbol{\omega}^h$ in each of the elements K_1 and K_2 will be,

$$\boldsymbol{u}^h = \mathbf{N}_e \mathbf{a}_e \qquad \boldsymbol{\omega}^h = \mathbf{N}_e \mathbf{b}_e \qquad \text{in } \tilde{\Omega}, \tag{3.25}$$

$$\boldsymbol{\varepsilon}^h = \nabla^s \boldsymbol{u}^h = \mathbf{B}_e \mathbf{a}_e \qquad \nabla^s \boldsymbol{\omega}^h = \mathbf{B}_e \mathbf{b}_e \qquad \text{in } \tilde{\Omega}, \tag{3.26}$$

where the index e stands for the element number. In vector $\mathbf{a}_e$ the nodal displacements, and in $\mathbf{b}_e$ the trial nodal displacement are found for each of the nodes of the two elements of figure 3.1. Note that the space where the shape and the weight functions come from is the same, considering of course the special requirements on the weight and trial functions where Dirichlet boundary conditions are applied. This is a particular property of the Galerkin methods, or more specifically, the Bubnov-Galerkin methods [11].

The jump and the average operators appearing in the weak form, are discretized as,

$$\left[\!\left[\boldsymbol{u}^h\right]\!\right] = \mathbf{N}_o^{[\![\,]\!]} \mathbf{a}_o \qquad \left[\!\left[\boldsymbol{\omega}^h\right]\!\right] = \mathbf{N}_o^{[\![\,]\!]} \mathbf{b}_o \qquad \text{on } \tilde{\Gamma}, \tag{3.27}$$

$$\left\{\mathbf{C} : \nabla^s \boldsymbol{u}^h\right\} \boldsymbol{n}_K = \mathbf{B}_o^{\{\,\}} \mathbf{a}_o \qquad \left\{\mathbf{C} : \nabla^s \boldsymbol{\omega}^h\right\} \boldsymbol{n}_K = \mathbf{B}_o^{\{\,\}} \mathbf{b}_o \qquad \text{on } \tilde{\Gamma}, \tag{3.28}$$

where the index o refers to the interior boundary. Vectors $\mathbf{a}_o$ and $\mathbf{b}_o$ are expressing again nodal displacement and trial displacements. However, now, the nodal and trial displacements of both elements at both sides of the interior edge are considered,

$$\mathbf{a}_o = \begin{bmatrix} \mathbf{a}_{e_1} \\ \mathbf{a}_{e_2} \end{bmatrix} \qquad \mathbf{b}_o = \begin{bmatrix} \mathbf{b}_{e_1} \\ \mathbf{b}_{e_2} \end{bmatrix}. \tag{3.29}$$

Back to the weak form of the interior penalty method, in equation (3.14), and replacing

equations in (3.25)–(3.28),

$$\int_{K_1} (\mathbf{B}_{e_1}\mathbf{b}_{e_1})^T \mathbf{C}\, \mathbf{B}_{e_1}\mathbf{a}_{e_1}\, d\Omega + \int_{K_2} (\mathbf{B}_{e_2}\mathbf{b}_{e_2})^T \mathbf{C}\, \mathbf{B}_{e_2}\mathbf{a}_{e_2}\, d\Omega - \int_{\tilde{\Gamma}} \left(\mathbf{B}_o^{\{\,\}}\mathbf{b}_o\right)^T \mathbf{N}_o^{[\![\,]\!]}\mathbf{a}_o\, d\Gamma$$
$$- \int_{\tilde{\Gamma}} \left(\mathbf{N}_o^{[\![\,]\!]}\mathbf{b}_o\right)^T \mathbf{B}_o^{\{\,\}}\mathbf{a}_o\, d\Gamma + \int_{\tilde{\Gamma}} \left(\mathbf{N}_o^{[\![\,]\!]}\mathbf{b}_o\right)^T \frac{\eta_K}{h_K}\boldsymbol{D}\, \mathbf{N}_o^{[\![\,]\!]}\mathbf{a}_o\, d\Gamma$$
$$= \int_{K_1} (\mathbf{N}_{e_1}\mathbf{b}_{e_1})^T \boldsymbol{f} d\Omega + \int_{K_2} (\mathbf{N}_{e_2}\mathbf{b}_{e_2})^T \boldsymbol{f} d\Omega + \int_{\Gamma^N} (\mathbf{N}_e\mathbf{b}_e)^T \boldsymbol{g}^N d\Gamma. \quad (3.30)$$

Because $\mathbf{b}_o$ is an arbitrary value, and considering (3.29), $\mathbf{b}_o$ can be canceled out,

$$\int_{K_1} \mathbf{B}_{e_1}^T \mathbf{C}\, \mathbf{B}_{e_1} d\Omega\, \mathbf{a}_{e_1} + \int_{K_2} \mathbf{B}_{e_2}^T \mathbf{C}\, \mathbf{B}_{e_2} d\Omega\, \mathbf{a}_{e_2} - \int_{\tilde{\Gamma}} \left(\mathbf{B}_o^{\{\,\}}\right)^T \mathbf{N}_o^{[\![\,]\!]} d\Gamma\, \mathbf{a}_o$$
$$- \int_{\tilde{\Gamma}} \left(\mathbf{N}_o^{[\![\,]\!]}\right)^T \mathbf{B}_o^{\{\,\}} d\Gamma\, \mathbf{a}_o + \int_{\tilde{\Gamma}} \left(\mathbf{N}_o^{[\![\,]\!]}\right)^T \frac{\eta_K}{h_K}\boldsymbol{D}\, \mathbf{N}_o^{[\![\,]\!]} d\Gamma\, \mathbf{a}_o$$
$$= \int_{K_1} (\mathbf{N}_{e_1})^T \boldsymbol{f} d\Omega + \int_{K_2} (\mathbf{N}_{e_2})^T \boldsymbol{f} d\Omega + \int_{\Gamma^N} \mathbf{N}_e^T \boldsymbol{g}^N d\Gamma. \quad (3.31)$$

Setting,

$$\mathbf{K}_o = \begin{bmatrix} \int_{K_1} \mathbf{B}_{e_1}^T \mathbf{C}\, \mathbf{B}_{e_1} d\Omega \\ \int_{K_2} \mathbf{B}_{e_2}^T \mathbf{C}\, \mathbf{B}_{e_2} d\Omega \end{bmatrix} - \int_{\tilde{\Gamma}} \left(\mathbf{B}_o^{\{\,\}}\right)^T \mathbf{N}_o^{[\![\,]\!]} d\Gamma - \int_{\tilde{\Gamma}} \left(\mathbf{N}_o^{[\![\,]\!]}\right)^T \mathbf{B}_o^{\{\,\}} d\Gamma$$
$$+ \int_{\tilde{\Gamma}} \left(\mathbf{N}_o^{[\![\,]\!]}\right)^T \frac{\eta_K}{h_K}\boldsymbol{D}\, \mathbf{N}_o^{[\![\,]\!]} d\Gamma, \quad (3.32)$$

$$\mathbf{f}_o = \begin{bmatrix} \int_{K_1} (\mathbf{N}_{e_1})^T \boldsymbol{f} d\Omega \\ \int_{K_2} (\mathbf{N}_{e_2})^T \boldsymbol{f} d\Omega \end{bmatrix} + \int_{\Gamma^N} \mathbf{N}_e^T \boldsymbol{g}^N d\Gamma, \quad (3.33)$$

the system to be solved for the elasticity case is finally,

$$\mathbf{K}_o\, \mathbf{a}_o = \mathbf{f}_o. \quad (3.34)$$

One dimension elements

The vectors $\mathbf{N}_e$ and $\mathbf{B}_e$, used in cG methods, as well as the vectors $\mathbf{N}_o^{[\![\,]\!]}$ and $\mathbf{B}_o^{\{\,\}}$ corresponding to the jump and average are defined hereinafter for the one dimensional linear elements case, figure 3.2(a),

$$\mathbf{N}_e = \begin{bmatrix} N_1 & N_2 \end{bmatrix} \qquad \mathbf{N}_o^{[\![\,]\!]} = \begin{bmatrix} N_1 & N_2 & -N_3 & -N_4 \end{bmatrix}_{\tilde{\Gamma}}, \quad (3.35)$$

$$\mathbf{B}_e = \begin{bmatrix} N_{1,x} & N_{2,x} \end{bmatrix} \qquad \mathbf{B}_o^{\{\,\}} = \frac{1}{2}EA \begin{bmatrix} N_{1,x} & N_{2,x} & N_{3,x} & N_{4,x} \end{bmatrix}_{\tilde{\Gamma}}, \quad (3.36)$$

where E stands for the elastic modulus and A the cross-sectional area. For quadratic elements, see figure 3.2(b),

$$\mathbf{N}_e = \begin{bmatrix} N_1 & N_2 & N_3 \end{bmatrix} \qquad \mathbf{N}_o^{[\![\,]\!]} = \begin{bmatrix} N_1 & N_2 & N_3 & -N_4 & -N_5 & -N_6 \end{bmatrix}_{\tilde{\Gamma}}, \quad (3.37)$$

$$\mathbf{B}_e = \begin{bmatrix} N_{1,x} & N_{2,x} & N_{3,x} \end{bmatrix} \quad \mathbf{B}_o^{\{\,\}} = \frac{1}{2}EA \begin{bmatrix} N_{1,x} & N_{2,x} & N_{3,x} & N_{4,x} & N_{5,x} & N_{6,x} \end{bmatrix}_{\tilde{\Gamma}}. \quad (3.38)$$

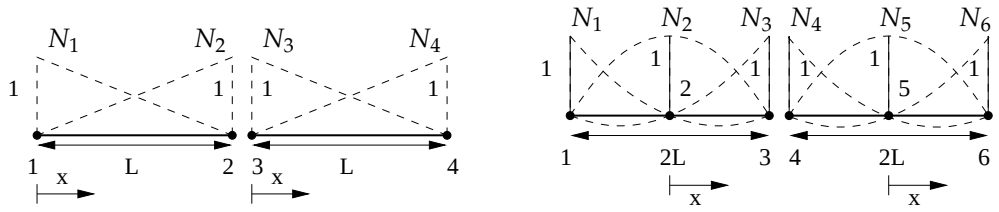

(a) Linear shape functions.

(b) Quadratic shape functions.

Figure 3.2. One dimension shape functions.

The choice of $\boldsymbol{C}$ will be taken equal to,

$$\boldsymbol{C} = EA, \tag{3.39}$$

as well as $\boldsymbol{D}$,

$$\boldsymbol{D} = EA, \tag{3.40}$$

to guarantee the dimensional consistency of the stability term.

Two dimensions case

For two dimensions Q4 elements, figure 3.1, $\mathbf{N}_e$ and $\mathbf{B}_e$ as in the continuous case, are equal to,

$$\mathbf{N}_e = \begin{bmatrix} N_1 & 0 & N_2 & 0 & N_3 & 0 & N_4 & 0 \\ 0 & N_1 & 0 & N_2 & 0 & N_3 & 0 & N_4 \end{bmatrix}, \tag{3.41}$$

$$\mathbf{B}_e = \begin{bmatrix} N_{1,x} & 0 & N_{2,x} & 0 & N_{3,x} & 0 & N_{4,x} & 0 \\ 0 & N_{1,y} & 0 & N_{2,y} & 0 & N_{3,y} & 0 & N_{4,y} \\ N_{1,y} & N_{1,x} & N_{2,y} & N_{2,x} & N_{3,y} & N_{3,x} & N_{4,y} & N_{4,x} \end{bmatrix}, \tag{3.42}$$

while the terms in the interior edges, [13], $\mathbf{N}_o^{[\![\,]\!]}$ and $\mathbf{B}_o^{\{\,\}}$, discussed in Appendix B, are,

$$\mathbf{N}_o^{[\![\,]\!]} = \begin{bmatrix} N_1 & 0 & \dots & N_4 & 0 & -N_5 & 0 & \dots & -N_8 & 0 \\ 0 & N_1 & \dots & 0 & N_4 & 0 & -N_5 & \dots & 0 & -N_8 \end{bmatrix}, \tag{3.43}$$

$$\begin{aligned} \mathbf{B}_o^{\{\,\}} = & \begin{bmatrix} C_{11}N_{1,x} & \dots & C_{11}N_{4,x} & C_{12}N_{4,y} & C_{11}N_{5,x} & C_{12}N_{5,y} & \dots & C_{12}N_{8,y} \\ C_{21}N_{1,x} & \dots & C_{21}N_{4,x} & C_{22}N_{4,y} & C_{21}N_{5,x} & C_{22}N_{5,y} & \dots & C_{22}N_{8,y} \end{bmatrix} \\ & + \begin{bmatrix} D_2N_{1,y} & \dots & D_2N_{4,y} & D_2N_{4,x} & D_2N_{5,y} & D_2N_{5,x} & \dots & D_2N_{8,x} \\ D_1N_{1,y} & \dots & D_1N_{4,y} & D_1N_{4,x} & D_1N_{5,y} & D_1N_{5,x} & \dots & D_1N_{8,x} \end{bmatrix}. \end{aligned} \tag{3.44}$$

being,

$$C_{11} = (\lambda + 2\mu)\ n_{K_1} \qquad C_{12} = \lambda\, n_{K_1} \qquad D_1 = \mu\, n_{K_1} \tag{3.45}$$

$$C_{21} = \lambda\, n_{K_2} \qquad C_{22} = (\lambda + 2\mu)\ n_{K_2} \qquad D_2 = \mu\, n_{K_2} \tag{3.46}$$

where λ and μ are the Lamé's constants. The choice of $\boldsymbol{D}$ for the two dimensional case will be taken equal to,

$$\boldsymbol{D} = \begin{bmatrix} E & 0 \\ 0 & E \end{bmatrix}. \tag{3.47}$$

3.6. Computer implementation

The computer implementation of the IP method is shown in Box 3.1. This procedure generally holds for other discontinuous Galerkin methods, just by changing the value of the local matrices obtained from the different choices of the numerical fluxes.

Step 1. Read problem and material data.

Step 2. Number global equations.

Step 3. Number interior edges.

Step 4. Allocate memory.

Step 5. Loop over the elements,
- 5.1 Form local stiffness matrix $\mathbf{K}_e$,
- 5.2 Form $\mathbf{f}_e$ vector,
- 5.3 Assemble $\mathbf{K}_e$ into global stiffness matrix $\mathbf{K}$,
- 5.4 Assemble $\mathbf{f}_e$ into RHS vector $\mathbf{f}$.

Step 6. Loop over the interior edges,
- 6.1 Form local constitutive matrix $\mathbf{K}_{\text{cons}}$,
- 6.2 Form local symmetry matrix $\mathbf{K}_{\text{sym}}$,
- 6.3 Form local stability matrix $\mathbf{K}_{\text{stab}}$,
- 6.4 Form local dG matrix $\mathbf{K}_o = \mathbf{K}_{\text{cons}} + \mathbf{K}_{\text{sym}} + \mathbf{K}_{\text{stab}}$,
- 6.5 Assemble $\mathbf{K}_o$ into global stiffness matrix $\mathbf{K}$.

Step 7. Add Neumann boundary conditions to $\mathbf{f}$.

Step 8. Solve the system of equations $\mathbf{K}\mathbf{u} = \mathbf{f}$.

Step 9. Postprocessing, calculate the stresses over $\tilde{\Omega}$ and on $\tilde{\Gamma}$.

Box 3.1: Implementation of the interior penalty method.

In Step 1 and for a discontinuous mesh, with no shared nodes between elements, every

element is totally independent from the rest. This freedom that characterizes discontinuous Galerkin methods make them ideally suited for *h*- and *p*-adaptivity. So *h*-refinement, by increasing the number of elements, can be done in a part of the mesh independently of other unchanged regions. *p*-refinement, by increasing for a fixed mesh the polynomial degree of the shape functions, can be done in some elements without worrying about the handling of hanging nodes. Another advantage that follows from this freedom is the possibility to combine independent meshes with a discontinuous interface mesh defined on their connecting boundary, and therefore analyze them easily as a single model.

This freedom has at the same time some negative consequences. The first one is that the number of nodes is increased, and therefore the size of the corresponding stiffness matrix. For the one dimensional linear case, and with the same number of elements, the size of the stiffness matrix for the discontinuous case is approximately twice the size of the continuous case, for the quadratic 1.5 times bigger while for two dimensions Q4 elements, it is four times bigger.

Another disadvantage is that the resulting stiffness matrix is more full. This comes from the fact that the matrices corresponding to the interior edges involve all nodes from two interfacing elements. This has consequences in the storage, where not only more capacity is needed due to the increased size of the matrix but also because of the fullness of the matrix. So for example, the storage capacity must increase two and a half times for the one dimensional linear case, 2.2 times for quadratic linear elements, and approximately six times for the Q4 two dimensional case.

In the Step 3 of Box 3.1, an algorithm is written that identifies and labels coinciding parts in space of interior edges corresponding to neighboring elements. That is, it must determine where the discontinuities are located and number them. This procedure is very time consuming since it has to go through the whole mesh identifying common edges.

This identification and numbering is then used in the Step 6 of Box 3.1. There, extra loops over each of the interior edges are used. Within each of these loops, $\mathbf{K}_o$ is evaluated over common nodes of two neighboring elements in the one dimensional case, or integrated over lines or surfaces for two and three dimensions respectively. These extra loops and the following evaluation or integration, compared to the continuous case, lead to more computational time.

In Step 9 of Box 3.1, the stress are calculated at each of the gauss points and in the interior edges. In the interior edges, $\tilde{\Gamma}$ and over Γ, use is made of the numerical fluxes definitions in (3.3) and (3.4) to calculate the stresses. So the stresses over $\tilde{\Gamma}$ and Γ will be calculated as,

$$\hat{\boldsymbol{\sigma}}\boldsymbol{n}_K = \left\{\mathbf{C} : \nabla^s \boldsymbol{u}^h\right\} \boldsymbol{n}_K - \boldsymbol{\mu} \left[\!\left[\boldsymbol{u}^h\right]\!\right] \qquad \text{on } \tilde{\Gamma} \cup \Gamma^D, \tag{3.48}$$

$$\hat{\boldsymbol{\sigma}}\boldsymbol{n}_K = \boldsymbol{g}^N \qquad \text{on } \Gamma^N. \tag{3.49}$$

To obtain an expression of the stresses over $\tilde{\Omega}$, equation (2.31) is again considered. The corresponding numerical fluxes for the IP are then introduced in equation (2.31) to obtain,

$$\int_{\tilde{\Omega}} \nabla^s \boldsymbol{\omega}^h : \boldsymbol{\sigma}^h d\Omega = \int_{\tilde{\Omega}} \nabla^s \boldsymbol{\omega}^h : \mathbf{C} : \nabla^s \boldsymbol{u}^h d\Omega - \int_{\tilde{\Gamma}} \left\{\nabla^s \boldsymbol{\omega}^h : \mathbf{C}\right\} \boldsymbol{n}_K \cdot \left[\!\left[\boldsymbol{u}^h\right]\!\right] d\Gamma. \tag{3.50}$$

Note that the stresses over $\tilde{\Omega}$ have a double component, one coming from the interior of the elements, $\boldsymbol{\sigma}^h_{\text{int}}$, and the other from the boundaries, $\boldsymbol{\sigma}^h_{\text{bound}}$. Introducing the lifting operator,

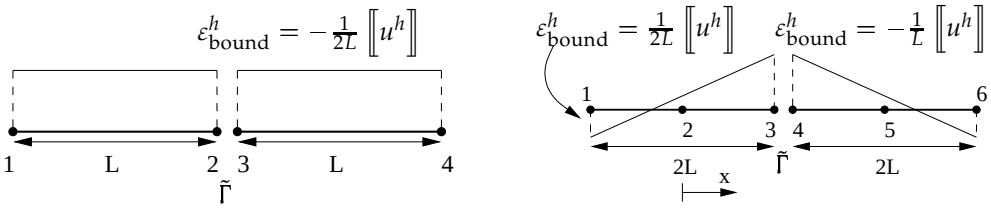

(a) $\varepsilon^h_{\text{bound}}$ for linear elements.

(b) $\varepsilon^h_{\text{bound}}$ for quadratic elements.

Figure 3.3. $\varepsilon^h_{\text{bound}}$ for the one dimensional case.

$\boldsymbol{R}(\cdot)$, defined in [8, 10], which transforms the integral on $\tilde{\Gamma}$ to an integral over $\tilde{\Omega}$,

$$-\int_{\tilde{\Gamma}} \left\{\nabla^s \boldsymbol{\omega}^h : \mathbf{C}\right\} \boldsymbol{n}_K \cdot \left[\!\left[\boldsymbol{u}^h\right]\!\right] d\Gamma = \int_{\tilde{\Omega}} \nabla^s \boldsymbol{\omega}^h : \mathbf{C} : \boldsymbol{R}\left(\left[\!\left[\boldsymbol{u}^h\right]\!\right]\right) d\Omega, \tag{3.51}$$

an expression of $\boldsymbol{\sigma}^h$ depending on the two mentioned components is obtained,

$$\boldsymbol{\sigma}^h = \boldsymbol{\sigma}^h_{\text{int}} + \boldsymbol{\sigma}^h_{\text{bound}} \qquad \text{in } \tilde{\Omega}, \tag{3.52}$$

where $\boldsymbol{\sigma}^h_{\text{int}}$ and $\boldsymbol{\sigma}^h_{\text{bound}}$ are defined as,

$$\boldsymbol{\sigma}^h_{\text{int}} = \mathbf{C} : \nabla^s \boldsymbol{u}^h \qquad \boldsymbol{\sigma}^h_{\text{bound}} = \mathbf{C} : \boldsymbol{R}\left(\left[\!\left[\boldsymbol{u}^h\right]\!\right]\right). \tag{3.53}$$

From equations (3.52) and (3.53) the double component of the strains for the IP method can be expressed as,

$$\boldsymbol{\varepsilon}^h = \boldsymbol{\varepsilon}^h_{\text{int}} + \boldsymbol{\varepsilon}^h_{\text{bound}}, \tag{3.54}$$

where,

$$\boldsymbol{\varepsilon}^h_{\text{int}} = \nabla^s \boldsymbol{u}^h \qquad \boldsymbol{\varepsilon}^h_{\text{bound}} = \boldsymbol{R}\left(\left[\!\left[\boldsymbol{u}^h\right]\!\right]\right). \tag{3.55}$$

For the one dimensional case, $\boldsymbol{\varepsilon}^h_{\text{bound}}$, can be expressed easily as a function of $\left[\!\left[u^h\right]\!\right]$. If linear elements are being used, it can be proved that the extra constant strain component, figure 3.3(a), added to the total strain is equal to,

$$\varepsilon^h_{\text{bound}} = -\frac{1}{2L}\left[\!\left[u^h\right]\!\right], \tag{3.56}$$

and for quadratic elements the extra linear stress is equal to, figure 3.3(b),

$$\varepsilon^h_{\text{bound}} = -\frac{1}{4L}\left[\!\left[u^h\right]\!\right]\left(\frac{3x}{L} + 1\right). \tag{3.57}$$

To calculate the extra component of the strain for the non-symmetric discontinuous Galerkin method the numerical fluxes in (3.17) and (3.18) are substituted into equation (2.31) as done for the IP method yielding,

$$\int_{\tilde{\Omega}} \nabla^s \boldsymbol{\omega}^h : \boldsymbol{\sigma}^h d\Omega = \int_{\tilde{\Omega}} \nabla^s \boldsymbol{\omega}^h : \mathbf{C} : \nabla^s \boldsymbol{u}^h d\Omega, \tag{3.58}$$

and since this holds for any $\boldsymbol{\omega}^h \in \mathcal{W}^h$,

$$\boldsymbol{\sigma}^h = \mathbf{C} : \nabla^s \boldsymbol{u}^h \qquad \text{in } \tilde{\Omega}. \tag{3.59}$$

The extra component of the strain is therefore, for the non-symmetric discontinuous Galerkin method, equal to,

$$\boldsymbol{R}\left(\left[\!\left[\boldsymbol{u}^h\right]\!\right]\right) = \mathbf{0}. \tag{3.60}$$

This difference lies in the choice of $\hat{\boldsymbol{u}}$. For the IP method the choice of $\hat{\boldsymbol{u}} = \left\{\boldsymbol{u}^h\right\}$ causes the appearance of the symmetry term and $\boldsymbol{R}\left(\left[\!\left[\boldsymbol{u}^h\right]\!\right]\right) \neq \mathbf{0}$. For the non-symmetric method, where $\hat{\boldsymbol{u}} = \boldsymbol{u}^h_{\partial K}$ is used, all the terms of equation (2.31) except the first of the left hand side and the first of the right hand side cancel out yielding equation (3.58) and finally equation (3.59).

3.7. Elasticity examples

In this section a one dimensional example will be given to analyze the convergence rate for the one dimensional case. An example for two dimensions plane strain will be shown as well.

3.7.1. Error analysis theory

The order of convergence determines how quickly the exact solution is approached upon mesh refinement. That is, how the error is reduced as the number of elements is increased. The numerical error is defined as,

$$\boldsymbol{e} = \boldsymbol{u} - \boldsymbol{u}^h, \tag{3.61}$$

where as stated before, $\boldsymbol{u}$ stands for the real solution and $\boldsymbol{u}^h$ for the approximate solution. To quantify the total error in displacements the Sobolev norm of order equal to zero is introduced as [11],

$$\left\|\boldsymbol{u} - \boldsymbol{u}^h\right\|_0 = \left(\int_\Omega (\boldsymbol{e}\cdot\boldsymbol{e})\ d\Omega\right)^{1/2}. \tag{3.62}$$

From the study of interpolating functions in combination with the projection properties of Galerkin methods [11], if the exact solution is smooth enough it yields,

$$\|\boldsymbol{e}\|_0 = C\, h_K^{p+1}\, \|\boldsymbol{u}\|_{p+1}, \tag{3.63}$$

where p stands for the polynomial order of the used shape functions, h_K is a measure of the element size and C is an unknown constant independent of h_K and $\boldsymbol{u}$. $\|\boldsymbol{u}\|_{p+1}$ represents the Sobolev norm of order $p+1$ of the real solution. This means that for the one dimensional case the order of convergence in terms of displacement is $O(h^2)$ using linear and $O(h^3)$ using quadratic elements.

To determine the rate of convergence in strains or stresses in the continuous Galerkin method the Sobolev norm of order equal to one is used,

$$\|\boldsymbol{e}\|_1 = C\, h_K^p\, \|\boldsymbol{u}\|_{p+1}\,, \tag{3.64}$$

being,

$$\|\boldsymbol{e}\|_1 = \left(\int_\Omega \left(\boldsymbol{e}\cdot\boldsymbol{e} + \nabla\boldsymbol{e} : \nabla\boldsymbol{e}\right)\, d\Omega\right)^{1/2}. \tag{3.65}$$

So for linear elements the order of convergence in strains or stresses is $O(h)$, and for quadratic elements $O(h^2)$.

According to [8], and as will be seen in this chapter, the previous expressions hold as well for dG methods through a proper choice of the penalizing parameter η_K.

Due to the discontinuity in displacements the value of $\nabla\boldsymbol{e}$ is not defined on the interior boundaries, $\tilde{\Gamma}$, and due to the existence of an extra strain component coming from the jump, $\|\boldsymbol{e}\|_1$ will be defined for the discontinuous case as,

$$\|\boldsymbol{e}\|_1 = \left(\int_{\tilde{\Omega}} \left(\boldsymbol{e}\cdot\boldsymbol{e} + \nabla\boldsymbol{e} : \nabla\boldsymbol{e} + \boldsymbol{R}\left(\left[\!\left[\boldsymbol{u}^h\right]\!\right]\right) : \boldsymbol{R}\left(\left[\!\left[\boldsymbol{u}^h\right]\!\right]\right)\right)\, d\Omega\right)^{1/2}, \tag{3.66}$$

where the value of $\boldsymbol{R}\left(\left[\!\left[\boldsymbol{u}^h\right]\!\right]\right)$ can be seen in equation (3.51) for the interior penalty method an in equation (3.60) for the non-symmetric discontinuous Galerkin method.

3.7.2. One dimensional example

In following sections results will be discussed for the interior penalty method and the non-symmetric discontinuous Galerkin method, defined in equation (3.19). The rate of convergence for each of these methods will be analyzed showing how it depends on η_K. A one dimensional example will be used with these two methods. This example can be seen in figure (3.4). The material and geometrical properties used are,

$$\begin{aligned} f(x) &= x^2\ N/m, \\ L &= 3\ m, \\ E &= 1\ N/m^2, \\ A &= 1\ m^2, \end{aligned} \tag{3.67}$$

and the analytical solution, expressed in m, for this case is equal to,

$$u = \frac{1}{12EA}\left(L^3 x - x^4\right). \tag{3.68}$$

Interior penalty method

In this section the convergence rate for the IP method will be examined considering the example of figure 3.4 with the geometrical and material properties appearing in equation 3.67. A separation will be made between the linear and the quadratic case.

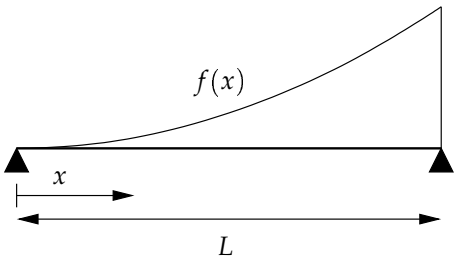

Figure 3.4. One dimensional numerical example.

In figure 3.5 the results are plotted for different number of linear elements, n_{el}, and stabilizing parameter η_k. In green the solution obtained with the IP method is shown. The continuous solution is drawn in red and the analytical solution in gray. For a value of $\eta_k = 0.9$, figure 3.5(a), the method is unstable because the minimum eigenvalue of the stiffness matrix becomes negative. In this case the system is still solvable, however for different number of elements and same value of η_K, problems might be faced due to the singularity of the system. That is it cannot be guaranteed that the system is solvable. If the number of elements is increased, see figure 3.5(b) the discontinuities between elements close as long as the choice of η_K, for the given number of elements, does not lead to a singular stiffness matrix. Just by a small increase of η_k, the method becomes stable, figure 3.5(c), and the analytical solution is approached. The jump on $\tilde{\Gamma}$ is reduced as the value of η_k is increased, figure 3.5(d).

The choice of $\hat{u} = \{u\}$ for the interior penalty method can be seen in figure 3.6, a detail of figure 3.5(d) for $x = 1.2\ m$, where the average of the displacement for the discontinuous case, green line, is equal to the value of the continuous case, in red, over $\tilde{\Gamma}$. This property can also be extended to the stresses, where it can be shown that the stresses over $\tilde{\Gamma}$, for the continuous case, can be obtained from the IP method by calculating $\sigma^h = E\left\{u^h_{,x}\right\} - E\frac{\eta_K}{h_K}\left[\!\left[u^h\right]\!\right]$. If the extra component of the stress coming from $\tilde{\Gamma}$, σ_{bound}, is added to what was called σ_{int} in the interior of the elements, exactly the same stresses are obtained using the IP method and traditional continuous Galerkin methods. The IP method is therefore, for the one dimensional case, nodally exact.

In figure 3.7(a) the displacement error and in 3.7(b) the error in stresses is shown for the IP method using linear elements. Note that for stable methods it leads to an optimal convergence rate. For an unstable method there is still convergence, however the rate is not guaranteed to be optimal. See as well how the convergence lines for the stresses in the continuous case and the discontinuous case, for values of η_K guaranteeing stability, lie in the same position since the stresses obtained with one or the other method are the same.

In figure 3.8 the displacement is plotted as in figure 3.5, but now using quadratic elements. Again in green the solution for the IP method is shown, in red for the cG method and in gray the analytical solution.

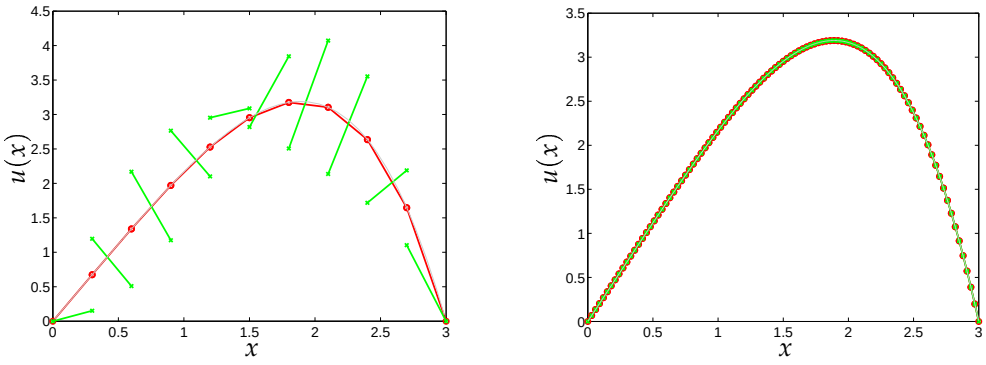

(a) $\eta_K = 0.9, n_{el} = 10.$

(b) $\eta_K = 0.9, n_{el} = 100.$

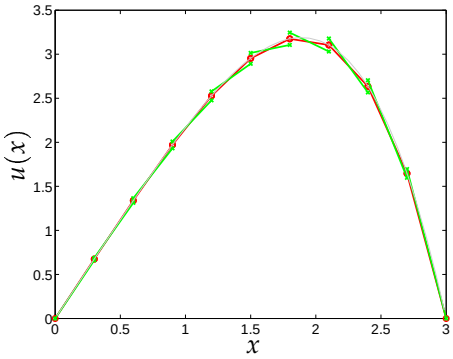

(c) $\eta_K = 1.1, n_{el} = 10.$

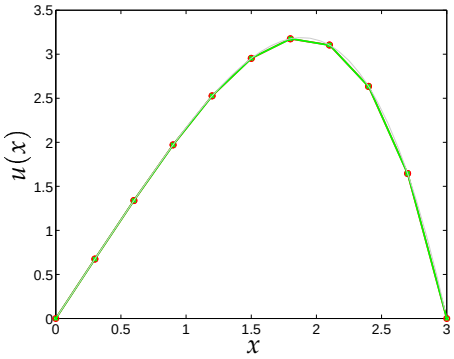

(d) $\eta_K = 5, n_{el} = 10.$

Figure 3.5. Interior penalty method with linear elements for different values of η_K.

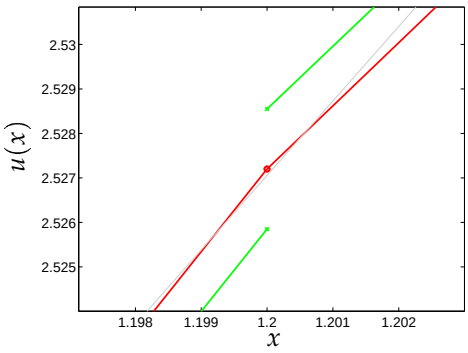

Figure 3.6. Detail of figure 3.5(d).

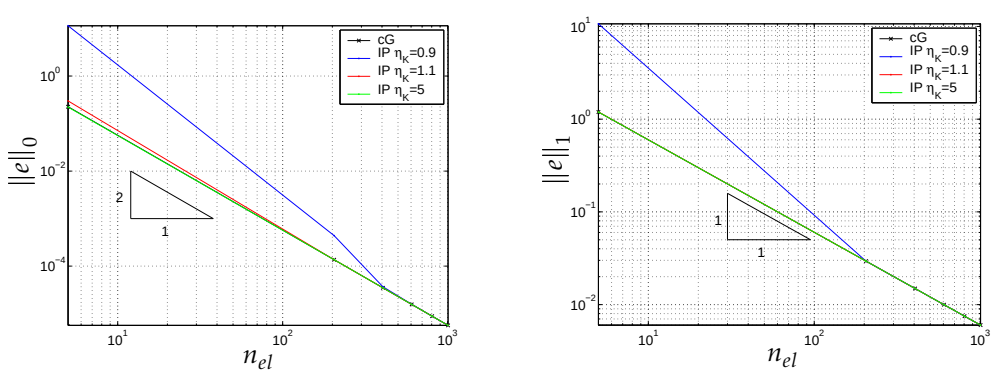

(a) Error in displacement.

(b) Error in stresses.

Figure 3.7. Error for interior penalty method using linear elements.

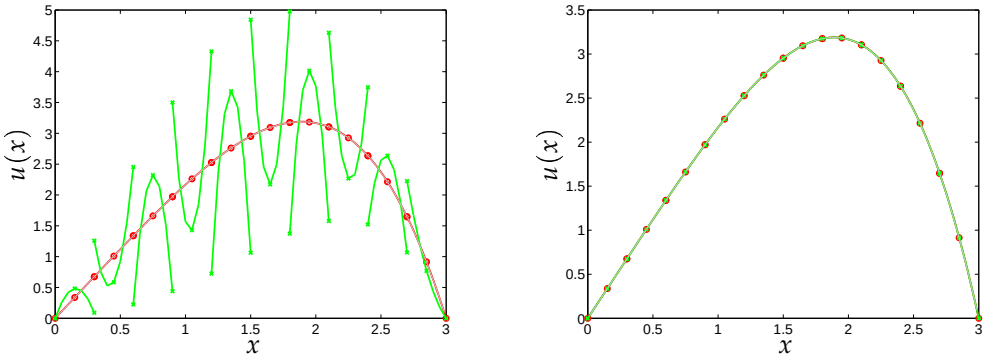

(a) $\eta_K = 2.95$, $n_{el} = 10$.

(b) $\eta_K = 3.1$, $n_{el} = 10$.

Figure 3.8. Interior penalty method with quadratic elements for different values of η_K.

Note how the value that guarantees stability for the quadratic case has changed. This value is located between 2.95, see figure 3.8(a), and 3.1, figure 3.8(b), for a bar of ten elements, while for the linear case it was located between 0.9, figure 3.5(a), and 1.1, figure 3.5(c) for the same number of elements.

For the one dimensional case using elements of equal length it is possible to determine a value of η_K which a priori ensures stability independently of the elastic modulus, cross-sectional area, element length and Neumann boundary conditions and only depending on the type of shape functions used. In figure 3.9 the value of this minimum η_K is shown for linear and quadratic shape functions. See that this value increases with the number of elements, but an upper bound can be found equal to one for the linear, and three for the quadratic case. So as long as η_K is taken greater than one or three, for the linear and quadratic case respectively, stability is guaranteed in the one dimensional elasticity case for the interior penalty method.

Again the choice of $\hat{u}$ can be seen in figure 3.10, which it is actually a detail of figure 3.8(b) for $x = 1.2\ m$. The same explained properties for the choice of $\hat{\sigma}$ hold now over $\bar{\Gamma}$. Again if $\boldsymbol{\sigma}^h_{\text{bound}}$ is added to $\boldsymbol{\sigma}^h_{\text{int}}$ the same stresses are found for the continuous Galerkin and the IP method.

In figure 3.11 the displacement and the stress error is shown for quadratic elements. Again stable methods yield maximum convergence rate.

Non-symmetric discontinuous Galerkin method

In this section the convergence rate of the non-symmetric discontinuous Galerkin, see equation (3.19), will be analyzed. This results in a consistent but not adjoint consistent non-symmetric method. The method is proved to be stable for values of $\eta_K > 0$.

The non-symmetric discontinuous Galerkin method converges for very low values of $\eta_K > 0$. It is seen in figure 3.12, that only after increasing the value of η_K the optimal

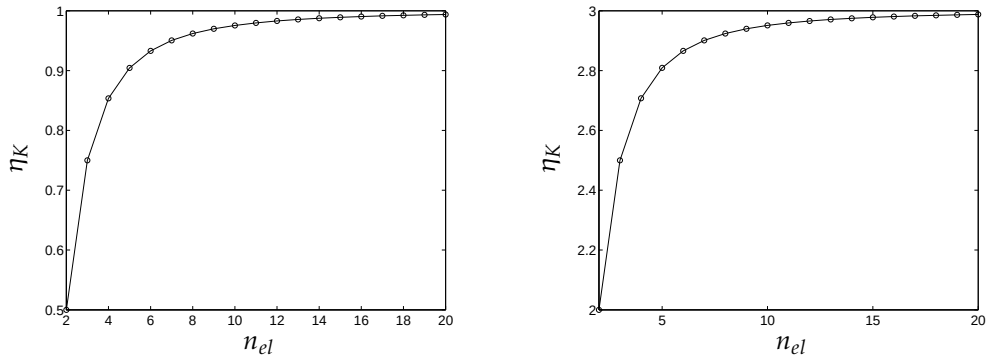

(a) Linear elements.

(b) Quadratic elements.

Figure 3.9. Minimum η_k guaranteeing stability for linear and quadratic one dimension shape functions for the interior penalty method.

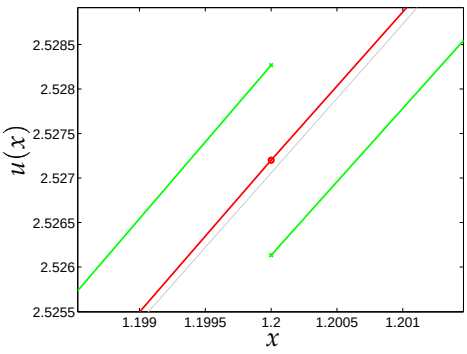

Figure 3.10. Detail of figure 3.8(b).

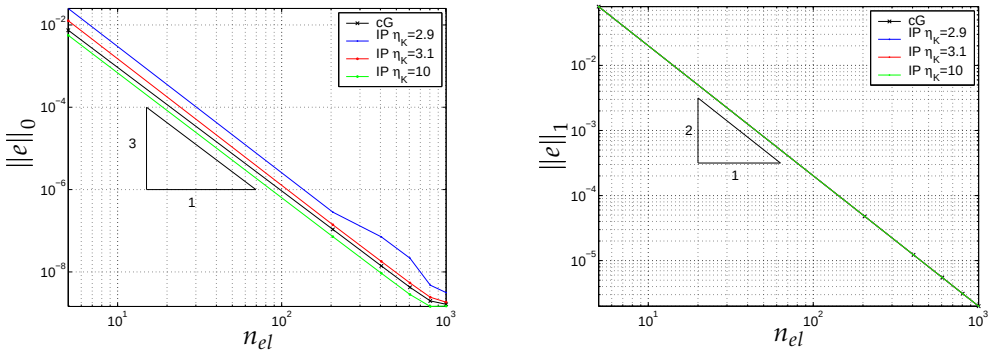

(a) Error in displacement.

(b) Error in stresses.

Figure 3.11. Error for interior penalty method using quadratic elements.

convergence rate is obtained for the displacements, while for stresses stable values of η_K lead to optimal convergence rate. According to Arnold [8] this is due the lack of adjoint consistency.

This method will be used in Chapter 4 since, as will be seen, its extension to the plasticity case is very simple, yielding a consistent and robust method. However, as has been said, it is not symmetric.

3.7.3. Two dimensional example

The performance of the two studied discontinuous Galerkin methods for the two dimensional plane strain case will be illustrated through the example given in figure 3.13. This consists of a plate loaded in the mid-section with the following geometrical and material properties,

$$\begin{aligned} F &= 5000\ N/mm, \\ L &= 1000\ mm, \\ h &= 50\ mm, \\ E &= 210000\ N/mm^2, \\ \nu &= 0.3. \end{aligned} \tag{3.69}$$

The solution obtained using the interior penalty method can be seen in figure 3.14. The deformation of the beam is shown in figure 3.14(a) and a detail of the midsection is seen in figure 3.14(b).

See how the IP method yields good results for the two dimensions case since the results obtained do not vary much for different stable values of η_K, figure 3.14(a). A simple relation from which obtain the displacements and the stresses for the continuous case as in the one dimensional case has not been found. The discontinuous nature of the method is shown in figure 3.14(b) where the discontinuity in the displacements is seen.

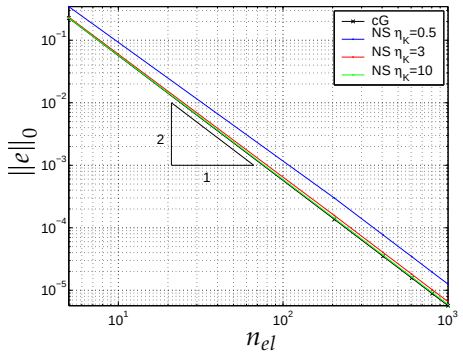

(a) Error in displacement using linear elements.

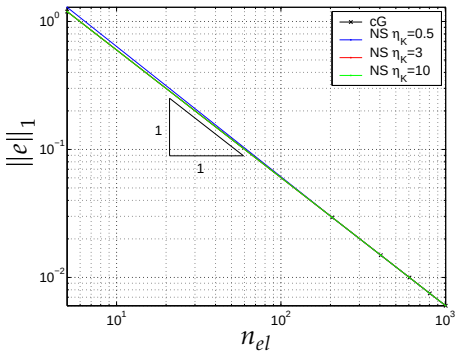

(b) Error in stresses using linear elements.

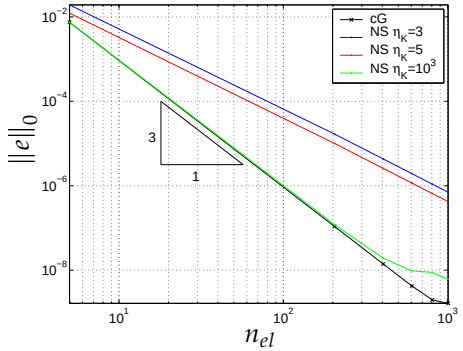

(c) Error in displacement using quadratic elements.

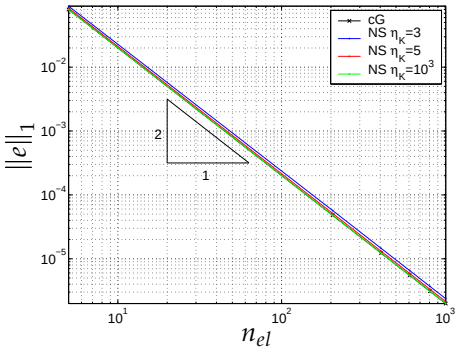

(d) Error in stresses using quadratic elements.

Figure 3.12. Error for non-symmetric method using linear and quadratic elements.

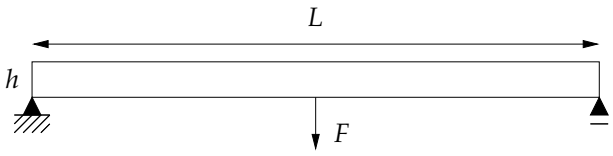

Figure 3.13. Two dimensional example.

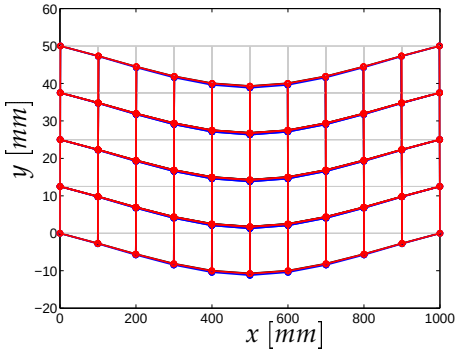

(a) Displacement of the beam in figure 3.13 using cG methods in black; IP with $\eta_K = 5$ in blue and in red $\eta_K = 100$.

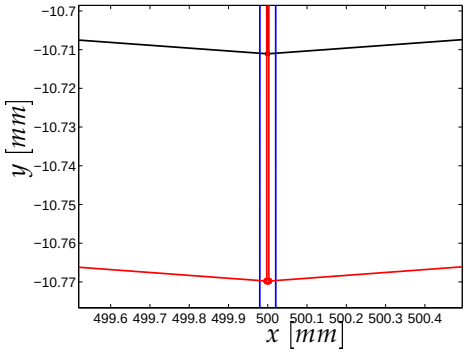

(b) Detail of displacement of the beam in figure 3.13 using cG methods in black; IP with $\eta_K = 5$ in blue and in red $\eta_K = 100$.

Figure 3.14. Two dimensions plane strain using the interior penalty method.

The results using the non-symmetric method are plotted in figure 3.15. The method is again consistent, see however that the displacements are bigger than in the IP method for the same value of η_K.

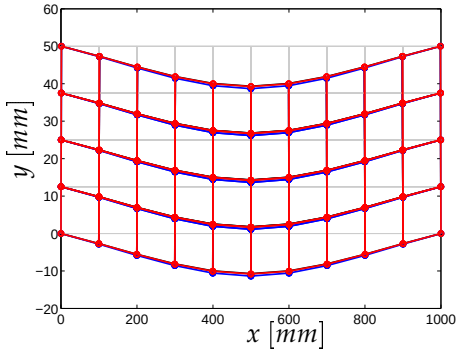

(a) Displacement of the beam in figure 3.13 using cG methods in black; NS with $\eta_K = 5$ in blue and in red $\eta_K = 100$.

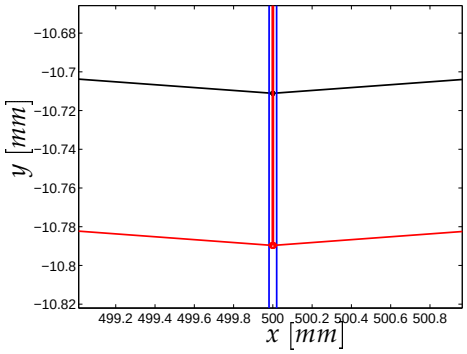

(b) Detail of displacement of the beam in figure 3.13 using cG methods in black;NS with $\eta_K = 5$ in blue and in red $\eta_K = 100$.

Figure 3.15. Two dimensions plane strain using the non-symmetric discontinuous Galerkin method.